Clim Dyn
DOI 10.1007/s00382-012-1383-3

Decadal variation of surface solar radiation in the Tibetan Plateau from observations, reanalysis and model simulations

Qinglong You · Arturo Sanchez-Lorenzo · Martin Wild · Doris Folini · Klaus Fraedrich · Guoyu Ren · Shichang Kang

Received: 4 February 2012 / Accepted: 23 April 2012

Abstract In this study, the annual and seasonal variations of all-sky and clear-sky surface solar radiation (SSR) in the eastern and central Tibetan Plateau (TP) during the period 1960–2009 are investigated, based on surface observational data, reanalyses and ensemble simulations with the global climate model ECHAM5-HAM. The mean annual all-sky SSR series shows a decreasing trend with a rate of -1.00 Wm^{-2} decade^{-1}, which is mainly seen in autumn and secondly in summer and winter. A stronger decrease of -2.80 Wm^{-2} decade^{-1} is found in the mean annual clear-sky SSR series, especially during winter and autumn. Overall, these results confirm a tendency towards a decrease of SSR in the TP during the last five decades. The comparisons with reanalysis show that both NCEP/NCAR and ERA-40 reanalyses do not capture the decadal variations of the all-sky and clear-sky SSR. This is probably due to a missing consideration of aerosols in the reanalysis assimilation model. The SSR simulated with the ECHAM5-HAM global climate model under both all-sky and clear-sky conditions reproduce the decrease seen in the surface observations, especially after 1980. The steadily increasing aerosol optical depth (AOD) at 550 nm over the TP in the ECHAM5-HAM results suggests transient aerosol emissions as a plausible cause.

Keywords Surface solar radiation · NCEP/NCAR · ERA-40 · ECHAM5-HAM · Tibetan Plateau

Q. You (✉) · S. Kang
Laboratory of Tibetan Environment Changes and Land Surface Processes, Institute of Tibetan Plateau Research, Chinese Academy of Sciences (CAS), Beijing 100085, China
e-mail: yqingl@126.com

Q. You · K. Fraedrich
Meteorological Institute, University of Hamburg, KlimaCampus, 21044 Hamburg, Germany

Q. You · G. Ren
Laboratory for Climate Studies, National Climate Center, China Meteorological Administration (CMA), Beijing 100081, China

A. Sanchez-Lorenzo · M. Wild · D. Folini
Institute for Atmospheric and Climate Science, ETH Zurich, Zurich, Switzerland
e-mail: arturo.sanchez@env.ethz.ch

M. Wild
e-mail: martin.wild@env.ethz.ch

D. Folini
e-mail: doris.folini@env.ethz.ch

S. Kang
State Key Laboratory of Cryospheric Science, Chinese Academy of Sciences (CAS), Lanzhou 730000, China

1 Introduction

Variations in solar radiation at the Earth's surface (or surface solar radiation, SSR), profoundly affect the human and terrestrial environment, which for example has significant implications for the intensity of the hydrological cycle, the carbon cycle, the cryosphere, and consequently for climate change scenarios. In recent decades, a decrease in SSR (also known as "global dimming") of about 7 Wm^{-2} was observed worldwide from the 1960s to 1980s at land stations and this topic has been widely studied (e.g. Gilgen et al. 1998; Liepert 2002; Stanhill and Cohen 2001; Qian et al. 2006, 2007; Kaiser and Qian 2002). More recent studies showed that the declining SSR faded during the 1980s, with an increase until the end of the twentieth century (also known as "brightening") (Wild et al. 2005). The SSR records suggest a continuation of the brightening after 2,000 at numerous stations in Europe and the United States, although with a renewed

Published online: 09 May 2012

decrease in some developing countries such as China or India (Wild et al. 2009). For a complete review of the subject see Wild (2009). In China, several studies have focused in the analysis of the SSR series, including their spatial and temporal patterns (e.g. Cha 1996; Li et al. 1998; Qian et al. 2006), data quality assessment (e.g. Shi et al. 2008; Tang et al. 2010), and causes of the observed changes (e.g. Xia et al. 2006; Qian et al. 2007).

The Tibetan Plateau (TP) with an average elevation of over 4,000 m a.s.l. and an area of approximately 2.5×10^6 km^2, is the highest and most extensive highland in the world. It has the largest area of snow and ice in the mid-latitudes and serves as "the world water tower" (Xu et al. 2008). The TP acts as water storage tower for South and East Asia, releasing melt water to the Indus, Ganges, Brahmaputra, and other river systems (Barnett et al. 2005; Immerzeel et al. 2010). However, the climate and cryosphere in the TP are undergoing rapid change (Kang et al. 2010), as seen in a significant warming or a weakening of wind speed (e.g. You et al. 2008a, b, 2010a, c). In a previous paper, the temporal variability of sunshine duration series in the TP has been analyzed (You et al. 2010b), and a significant decrease is shown since the 1980s. However, a systematic assessment of the long-term trends of all-sky and clear-sky SSR using surface observations, reanalyses and climate simulations over the TP is still lacking.

In this study, the annual and seasonal variations of SSR in the TP during the period 1960–2009 are investigated based on the available surface observational data as well as two reanalysis products. To better understand the variations in SSR and its causes in the TP, results of simulations performed with the global climate model ECHAM5-HAM are also analyzed.

2 Data and methods

2.1 Surface dataset

Daily SSR data from stations in the TP are provided by the National Meteorological Information Center, China Meteorological Administration (NMIC/CMA). The Chinese SSR dataset contains 20 stations within the domain of 26°–40°N and 73°–105°E, a window that covers the main area of the TP in China. Five stations (Kashi, Mianyang, Lijiang, Pazhihua, Emeishan) are excluded because their locations are away from the actual boundary of TP. At the same time, five stations with measurements starting in the 1990s are also not considered. The remaining 10 stations are selected for the homogenisation step. Table 1 shows the details of the SSR stations used in this study, with their World Meteorological Organization (WMO) number, name, longitude, latitude, elevation and missing data during the 1960–2009 period. The SSR measurement network in China began in 1957 in the framework of the 1957–1958 International Geophysical Year (Shi et al. 2008), and most of the stations initiated systematic SSR measurements after 1960. Consequently, this study covers the period from 1960 to 2009.

Shi et al. (2008) pioneered the systematic assessment of data quality of 122 SSR observations in China during 1957–2000. Tang et al. (2010) categorized the errors related to SSR measurements in China into two classes: one is caused by equipment errors and uncertainty, the other is due to operation-related problems and errors. The CMA performed some quality checks on the SSR data, which are affected by several factors such as accuracy and modification of instruments, artificial factors and location change. Shi et al. (2008) explained the calibration procedure in China: (1) calibration at least once per month at the stations against the reference instruments; (2) calibration of the reference radiometers against the regional reference instruments; (3) calibration of the regional reference instruments every 2 year against the Chinese reference instruments.

The homogenization of a dataset is a necessary step before trends can be calculated because erroneous data can seriously impact the trends. The homogeneity assessment and adjustment can be a complex process which often requires close neighbour stations and detailed station history, because inhomogeneities can be caused, for example, by changes in instrumentation, station relocations or changes in the local environment such as urbanization (Vincent et al. 2005). For the SSR dataset in the TP, a possible inhomogeneity due to changes in the instrumentation occurred in the early 1990s, when pyranometers were systematically replaced in the Chinese network. As summarized by Shi et al. (2008), before the early 1990s the instruments used to measure SSR were identical to the ones used in the former Soviet Union, named Yanishevsky thermoelectric pyranometer. Afterwards, the DFY-4 pyranometers manufactured in China were used to measure SSR. Unfortunately, no information about the exact year of change at each station is available to our knowledge. In fact, Shi et al. (2008) suggest a change in the pyranometers in the early 1990s, whereas Tang et al. (2011) assume this change in 1994 for all stations in China. Nevertheless, the former study (Shi et al. 2008) does not assume a systematic bias in the series as a consequence of the change (although a possible effect is not completely rejected). On the other hand, the latter study (Tang et al. 2011) suggests that a strong inhomogeneity occurred in all SSR series in 1994, assuming that the measurements before these years were non-reliable in China. Although their conclusion cannot be ruled out entirely, it seems implausible that this instrument change occurred at all Chinese stations at the same time. Equally, a change in the pyranometers cannot be considered as a cause of inhomogeneity per se, especially because

Table 1 Details of the 10 selected stations in the Tibetan Plateau, including the World Meteorological Organization (WMO) code, station name, latitude, longitude, elevation, and starting year of the SSR series, and data missing during the period 1960–2009

Code	Station	Lat. (N)	Lon. (E)	Alt. (m)	Starting year
51777	**Ruoqiang**	39.02	88.10	888	1957
51828	**Hetian**	37.08	79.56	1374	1957
52681	Minqin	38.38	103.05	1367	1961
52818	**Germu**	36.25	94.54	2807	1957
52866	Xining	36.43	101.45	2295	1959
55228	Geer	32.3	80.05	4278	1971
55299	Naqu	31.29	92.04	4507	1961
55591	Lhasa	29.4	91.08	3649	1961
56029	Yushu	33.01	97.01	3681	1960
56137	**Changdu**	31.09	97.1	3306	1961

The names of the 4 homogeneous SSR series are highlighted in bold

the estimated errors in SSR measurements for both types of instruments are similar (Shi et al. 2008). Further evidence for a non-common break due to the instrumental change in the Chinese SSR series during the early 1990s is shown by Wang et al. (2011, Fig. 3), where the mean seasonal SSR series in different regions of China suggest that a strong increase in the early 1990s can only be seen clearly in the mean series of the TP and South China (Wang et al. 2011), but not in the mean series of the other regions in China. Consequently, a widespread inhomogeneity of the SSR measurements in China during the period before 1992 cannot be assumed as a plausible phenomenon.

In the present study, the homogeneity of each of the 10 SSR series was checked by means of the Standard Normal Homogeneity Test (SNHT) (Alexandersson and Moberg 1997). Our procedure rejects the priori existence of homogenous reference series and consists of testing each of the 10 series against the other series. Note that in the homogenization produce some stations in the surroundings of the TP have been used (e.g. the Emeishan series that has been excluded from the SSR dataset as previously detailed), as they are highly correlated with some of the 10 selected series. When a break is identified in one series (test series), the series used to estimate the adjustments, which were calculated on a monthly basis, is chosen among the highest correlated series that prove to be homogeneous. The results confirm that 5 (Xining, Geer, Naqu, Lhasa and Yushu) of the 10 series (i.e. 50 % of the series) show evidence of inhomogeneities in the early 1990s, most of them clearly as a result of low values during the preceding 5–10 years, as has been previously pointed out by Shi et al. (2008). Another statistical inhomogeneity was detected in Minqin during the mid-1970s. The remaining 4 series (Ruoqiang, Hetian, Germu, Changdu) proved to be homogeneous (see Table 1). These 4 series have been used as reference series in order to estimate the corrections of the breaks identified in the inhomogeneous series. After the homogenization, all gaps were filled with monthly mean values for each station.

In order to study the trends under clear-sky SSR conditions, only the 4 stations considered as homogenous for all-sky SSR series are used (Sanchez-Lorenzo et al. 2009). Firstly, the daily mean total cloud cover records are obtained from the NMIC/CMA for these 4 series. Secondly, a day was defined as clear-sky if the daily mean total cloud cover is equal or less than 12.5 %. Finally, the clear-sky SSR monthly values for each station were obtained by averaging the SSR values of all clear-days available in each month.

2.2 NCEP/NCAR and ERA-40 reanalysis

In addition to the observed data, SSR fluxes as estimated by two reanalysis products are used in this study, i.e. the reanalysis from the National Centers for Environmental Prediction/National Center for Atmospheric Research (NCEP/NCAR) (Kalnay et al. 1996) and the reanalysis from the European Centre for Medium-Range Weather Forecasts (ECMWF) (ERA-40) (Uppala et al. 2005).

The NCEP/NCAR dataset covers the period from 1948 to present with a spatial resolution of 2.5° × 2.5° (Kalnay et al. 1996). Only data from 1960 to 2009 are analyzed in this study. The ERA-40 reanalysis is available from 1957 to mid-2002 with a spatial resolution of 2.5° × 2.5° (Uppala et al. 2005). Only data covering the 1960–2001 period are used in this study. As downward clear-sky SSR data is not directly available in ERA-40, we use net clear-sky SSR instead.

2.3 The ECHAM5-HAM model

The fourth data set we analyse are transient simulation data computed with the global climate model ECHAM5, developed at the Max Planck Institute of Meteorology (MPI), (Roeckner et al. 2003, 2006), coupled to the

Hamburg Aerosol Module (HAM) (Stier et al. 2006a) and equipped with detailed cloud microphysics (Lohmann et al. 2007). The ECHAM5-HAM is particularly well suited for the present study, as aerosol-cloud interactions are considered as a main factor in the explanation of the observed decadal variations in SSR (e.g. Ohmura 2009; Wild 2009).

In the present simulations, aerosol emissions are taken from the Japanese National Institute for Environmental Studies (NIES) (Roeckner et al. 2006; Stier et al. 2006b). Fossil fuel emissions of SO2, BC and OC are prescribed annually, while emissions from wild fires, agricultural burning and domestic fuel-wood consumption are prescribed monthly. Optical depths of volcanic aerosols in the stratosphere are prescribed on a monthly basis on six latitudinal bands. Total solar irradiance varies on an annual basis (Solanki and Krivova 2003). Monthly mean sea surface temperatures (SSTs) and sea ice concentrations (SICs) are taken from the Hadley Centre (Rayner et al. 2003). An ensemble of 13 experiments is performed at spectral resolution T42 (about 2.8 × 2.8 degrees), with 19 vertical levels from ground to 10 hPa, and covering the time period from 1870 to 2005. In recent studies, these simulation data have already been analysed on the global scale (Bichet et al. 2011) and for Europe (Folini and Wild 2011). Here, we look at the TP and focusing on the period 1960–2005.

3 Methods

Annual and seasonal series are computed from the monthly data previously described. In this study the seasons are defined as spring (MAM), summer (JJA), autumn (SON), and winter (DJF). The winter season was defined as the mean of the December of the year indicated and the January and February of the subsequent year.

Annual and seasonal anomalies, obtained as deviations from the 1971–2000 period, were calculated for each one of the 10 (4) series of observed all-sky (clear-sky) SSR. Mean series for the TP were computed as an arithmetic mean of these 10 (4) series for all-sky (clear-sky) SSR. The same approach has been applied for the reanalysis and ECHAM5-HAM simulations, but using the time series of the nearest grid point to the 10 (4) stations (see Fig. 1). Overall, the use of anomalies avoids the introduction of a bias in case of missing data and different absolute values, and the mean series enhances the signal-to-noise ratio, which permits a better identification of decadal trends than individual series.

The linear trends of all series in this paper were calculated by means of least squares linear fitting and their significance estimated by the Mann–Kendall nonparametric test (Sen 1968) at the 0.05 level of significance. In order to improve the visualization of the decadal variability, the mean time series are plotted together with their 17-year Gaussian low-pass filter (hereafter referred as 17GLPF), which only consider the values on one side at the start and end of the series in order to filter the full period of 1961–2009.

Finally, correlation analyses are used to compare the observed and simulated SSR series. All correlations are based on the mean time series smoothed with the 17GLPF in order to evaluate the agreement in the decadal variability rather than the interannual variations which are not deterministic in global climate models.

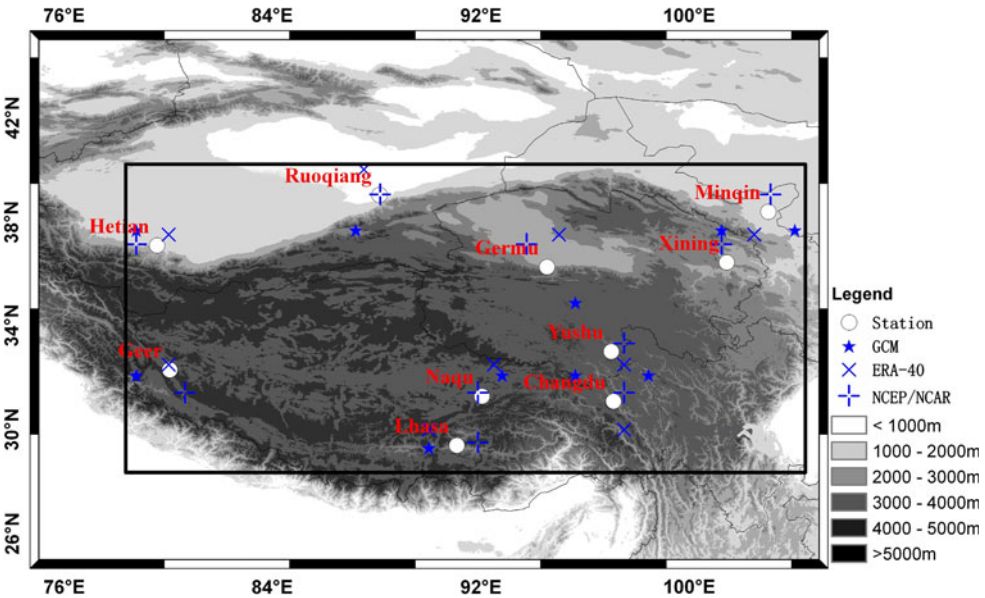

Fig. 1 Distribution of the 10 stations with SSR measurements and the corresponding nearest reanalysis and ECHAM-HAM grid points in the Tibetan Plateau

4 Results

4.1 Changes of all-sky and clear-sky SSR from observational data

The climatological means for all-sky SSR on annual and seasonal basis are summarized in Table 2. The annual mean all-sky SSR value, obtained by averaging the 10 series available in the TP, is 210.1 Wm^{-2}, with a clear maximum in summer (263.1 Wm^{-2}) and minimum in winter (143.4 Wm^{-2}).

Figure 2 shows the mean annual and seasonal all-sky SSR series in the TP during the period 1960–2009. The linear trends for the all-sky SSR series, calculated over the whole available period (1960–2009) and different subperiods, are summarized in Table 3. On the annual basis, the mean all-sky SSR series in the TP shows an increasing tendency before the 1970s, followed by a decrease during the 1970–1990 period. Subsequently, the series shows a new increase in the 1990s, followed by a strong decrease during the first decade of the new century. Totally, the all-sky SSR exhibits a significant decreasing trend for the whole study period with a rate of -1.00 Wm^{-2} $decade^{-1}$. Equally, both the 1960–1992 and 1993–2009 subperiods show a significant decrease of -1.68 and -5.48 Wm^{-2} $decade^{-1}$, respectively. The trends of these subperiods confirm a tendency towards a decrease before and after 1992, the year with the possible inhomogeneity remaining in the series due to the instrumentation change. On a seasonal basis, the results highlight a general decrease in all-sky SSR, with the highest rate of significant decrease found in autumn (-2.16 Wm^{-2} $decade^{-1}$), followed by summer (-1.26 Wm^{-2} $decade^{-1}$) and winter (-1.09 Wm^{-2} $decade^{-1}$), and a non-significant increase in spring (Table 3).

Figure 3 shows the mean annual and seasonal clear-sky SSR series in the TP during the studied period, based on the 4 homogeneous stations. Trends in clear-sky SSR for different subperiods are shown in Table 3. In contrast to all-sky SSR, the annual clear-sky SSR series starts with two decades without relevant variations, followed by a sharp decrease during 1982–1984. Afterwards, there is a slight recovery between mid-1980s and the beginning of 2000, only interrupted by another strong decrease during the 1991–1992, ending with a clear decrease during the final years. Regarding long-term trends over the 1961–2009 period, the clear-sky SSR annual series shows a significant decrease of -2.80 Wm^{-2} $decade^{-1}$, caused mainly by a decrease in winter (-4.45 Wm^{-2} $decade^{-1}$) and autumn (-3.78 Wm^{-2} $decade^{-1}$). The largest decreasing trend occurs in the subperiod of 1993–2009 (-11.40 Wm^{-2} $decade^{-1}$). In most cases, it becomes evident that the SSR trends under all-sky conditions are slightly smaller than under clear-sky conditions, both on annual and seasonal basis (Table 3).

Table 3 also contains the trends of the mean all-sky SSR series if only the 4 series used for the clear-sky analysis are considered. The results show a tendency toward larger linear trends with the subset of the 4 series, although the main features remain fundamentally unchanged. The strong spatial autocorrelation in the SSR series, as illustrated with the correlation of 0.87 between these smoothed annual all-sky SSR series, suggests a similar decadal variability when the 4 series rather than the 10 series are considered.

4.2 Changes of all-sky and clear-sky SSR from reanalysis data

For the NCEP/NCAR reanalysis, the climatological mean of all-sky SSR (Table 2) tends to be higher than the observational stations, with an annual value of 275.9 Wm^{-2} (bias of +31.3 % with respect to the observations), which is in line with the differences found by in the middle reaches of the Yangtze River (Xia et al. 2006). A similar overestimation is found throughout the seasons, with the largest bias in spring (+36.9 %). For the ERA-40, the climatological mean all-sky SSR (Table 2) is smaller than the NCEP/NCAR, and closer to the surface observations, with a slight positive bias (+0.6 %) on the annual basis, whereas an overestimation (underestimation) around 5–10 % is found in spring and winter (summer and autumn).

Table 2 Annual and seasonal mean of all-sky SSR in the TP as observed, determined in reanalyses (NCEP/NCAR and ERA40) and simulated by the ECHAM5-HAM

	Annual	Spring	Summer	Autumn	Winter
Observations all-sky SSR	210.1	243.0	263.1	191.1	143.4
NCEP/NCAR all-sky SSR	275.9 (+31.3)	332.7 (+36.9)	339.3 (+29.0)	239.8 (+25.5)	192.2 (+34.0)
ERA-40 all-sky SSR	211.5 (+0.7)	268.0 (+10.3)	247.0 (−6.1)	180.1 (−5.8)	151.4 (+5.6)
ECHAM5-HAM all-sky	203.7 (−3.0)	239.8 (−1.3)	246.7 (−6.2)	184.3 (−3.6)	144.0 (+0.4)

Units are Wm^{-2}, and the reference period used is 1971–2000. For the mean calculations only the 10 stations (nearest grid point to the station) are used for the observations (reanalyses and ECHAM5-HAM simulations). Relative differences (%) with respect to the observations are given in parentheses

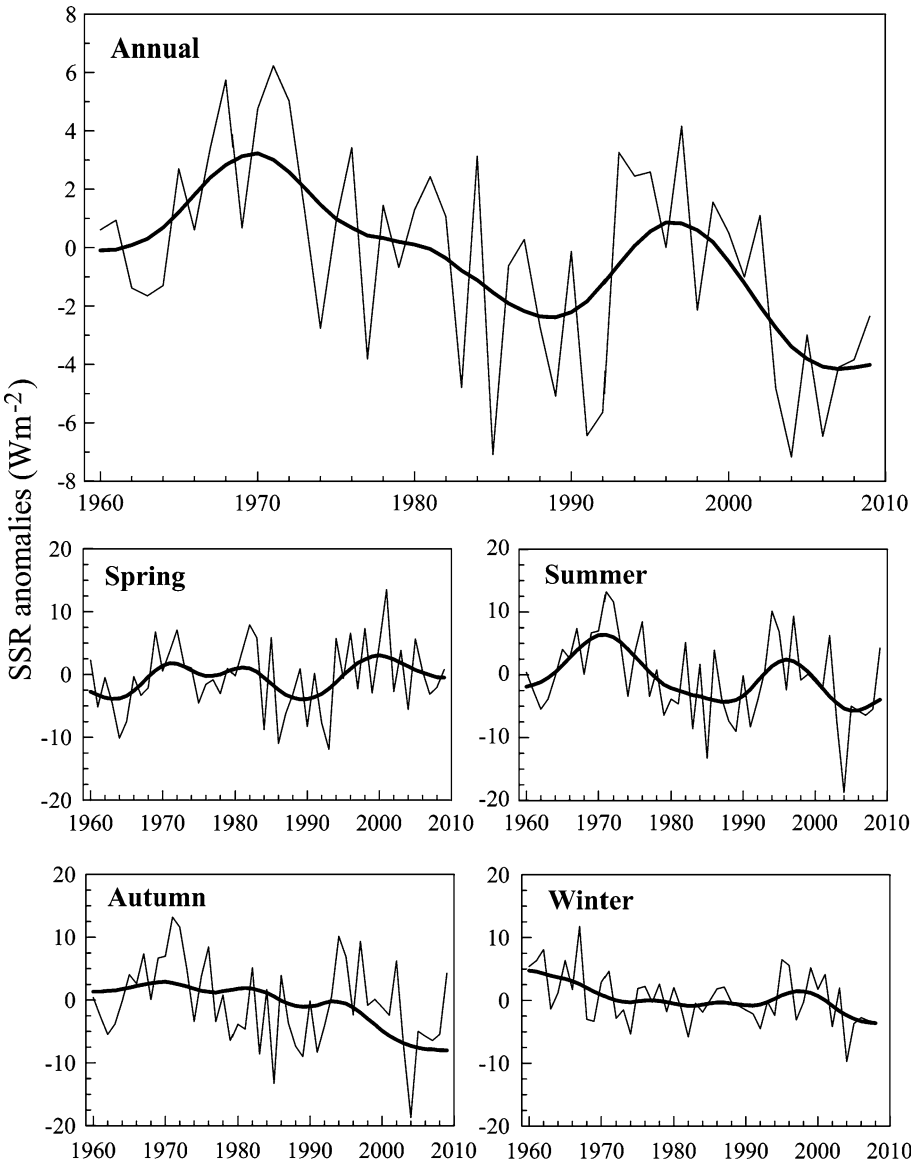

Fig. 2 Mean annual and seasonal all-sky SSR series (*thin line*) in the Tibetan Plateau during the period 1960–2009, plotted together with a GLPF17 (*thick line*). The series are expressed as differences (anomalies in Wm^{-2}) relative to the 1971–2000 reference period

Table 3 Linear trends in the mean Tibetan Plateau (TP) all-sky and clear-sky SSR observational series, given as Wm^{-2} $decade^{-1}$

	Annual	Spring	Summer	Autumn	Winter
Obs. all-sky, 1960–2009	−1.00* (−2.09)	0.52 (−1.02)	−1.26* (−2.25*)	−2.16* (−2.40)	−1.09* (−2.56*)
Obs. all-sky, 1960–1992	−1.68* (−3.14*)	−0.31 (−3.48*)	−2.61* (−3.75*)	−1.37 (−2.21*)	−2.01* (−2.97*)
Obs. all-sky, 1993–2009	−5.48* (−5.50)	0.02 (−1.50)	−7.24* (−8.02)	−8.27* (−8.34*)	−4.5 (−5.77)
Obs. all-sky, 1993–2005	−6.83* (−6.01)	3.73 (4.76)	−12.81* (−15.76*)	−11.26* (−11.42*)	−4.86 (−5.53)
Obs. clear-sky, 1960–2009	−2.80*	−1.81	−1.22	−3.78*	−4.45*
Obs. clear-sky, 1960–1992	−4.76*	−5.48*	−2.91	−5.65*	−4.84*
Obs. clear-sky, 1993–2009	−11.40*	−14.85*	−14.68*	−8.56	−7.46*
Obs. clear-sky, 1993–2005	−11.73	−11.09	−22.18*	−9.72	−4.00

The trends are shown for the 1960–2009, 1960–1992, 1993–2009 and 1993–2005 periods. Trends values of the mean TP all-sky SSR only considering the 4 homogeneous series are given in parentheses

* Significant at the 0.05 level

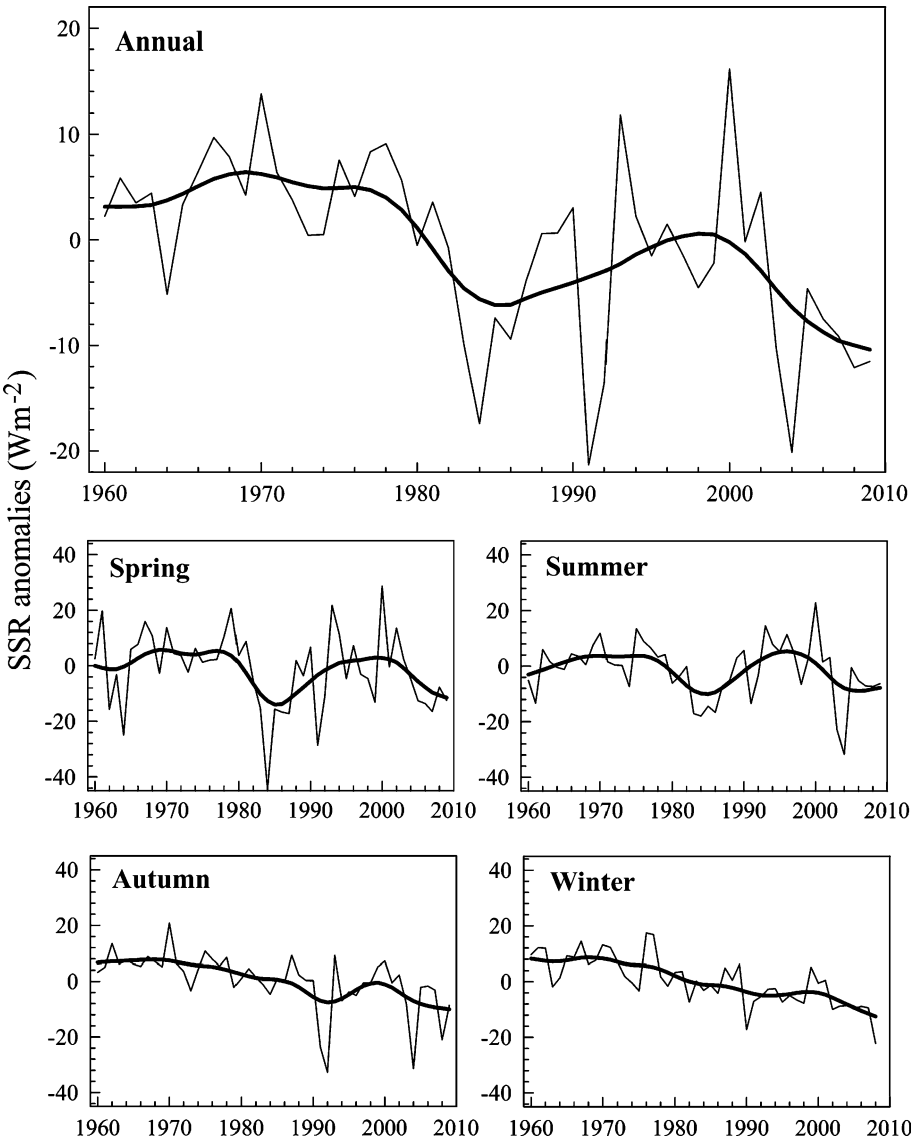

Fig. 3 As Fig. 2, but for clear-sky SSR observational series in the Tibetan Plateau. The mean series are constructed only considering the SSR and TCC daily records of the 4 homogeneous series. A day is defined as clear if the TCC daily mean is less than 1 okta

Figure 4 (top) shows the annual mean all-sky SSR series from NCEP/NCAR and ERA-40 in the TP composed from the grid points closes to the 10 stations. The annual all-sky SSR mean series from NCEP/NCAR shows a tendency towards a decrease before 1970 and during the 1980s, and an increasing trend during the 1970s and the 1990s and turns to decrease after that. The annual all-sky SSR has an increasing trend with a rate of 1.06 Wm^{-2} $decade^{-1}$ during the period 1960–2009. On the other hand, the mean annual all-sky SSR series from the ERA-40 shows a decrease before 1970 and after 1980 and increases during the 1970s and 1980s. The linear trend, estimated over the 1960–2004 period, is slightly positive, but not significant. The time variability and trends of all-sky SSR on a seasonal basis show similar features to the annual series for both reanalysis (not shown).

Figure 4 (bottom) shows the mean annual clear-sky (net clear-sky) SSR series from NCEP/NCAR (ERA-40) in the TP. Clear-sky SSR series from NCEP/NCAR show a slight but significant increase (0.17 Wm^{-2} $decade^{-1}$) during the whole period. The seasonal anomalies series show similar features and the largest trend magnitude is found in spring (not shown). For the ERA-40, the mean annual clear-sky net SSR series has a sharp decrease before the 1970s followed by a period without relevant variations up to the present, with a significant decrease (-0.91 Wm^{-2} $decade^{-1}$) during the whole period 1960–2001, and with the largest seasonal trend in spring (not shown).

Overall, the all-sky and clear-sky SSR trends derived from both NCEP/NCAR and ERA-40 cannot capture the decadal variations seen in surface observations in the TP.

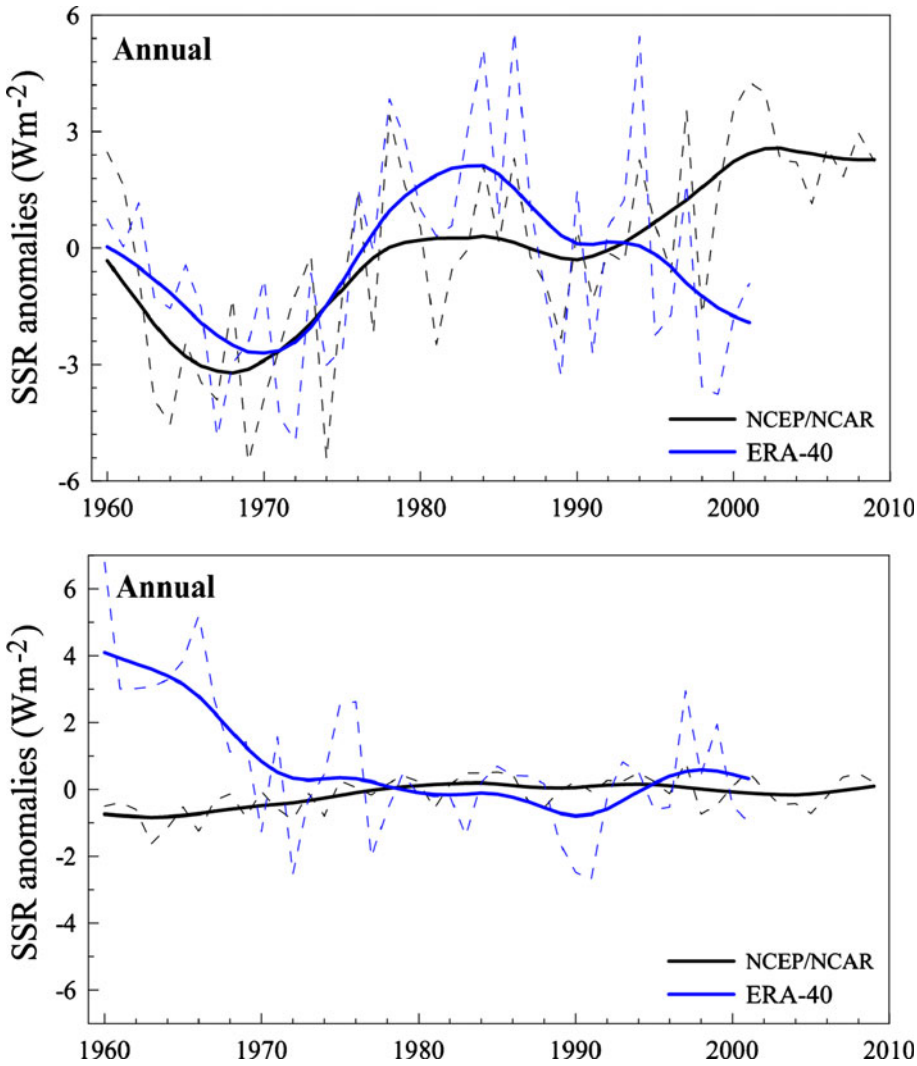

Fig. 4 Mean annual (*top*) all-sky and (*bottom*) clear-sky SSR series (*thin dashed lines*) in the Tibetan Plateau for the NCEP/NCAR (in *black*) and ERA-40 (in *blue*) reanalyses, together with a GLPD17 (*thick solid lines*), during the 1960–2009 and 1960–2001 period, respectively. The series are expressed as differences (anomalies in Wm^{-2}) relative to the 1971–2000 reference period, and are calculated using the nearest grid points to the 10 (4) surface stations with all-sky (clear-sky) SSR series

4.3 Changes of simulated all-sky and clear-sky ensemble SSR by ECHAM5-HAM

Figures 5 and 6 show the annual and seasonal all-sky and clear-sky ensemble mean SSR series from ECHAM5-HAM simulations for the TP from 1960 to 2005. The means and trends of these values are summarized in Tables 2 and 4. For comparison, Table 3 also shows trends covering the 1993–2005 subperiod in the observational series.

The climatological mean of the annual mean ensemble SSR from the ECHAM5-HAM at all-sky condition is 203.7 Wm^{-2}, which is slightly lower than both the surface observations (−3.0 %) and reanalysis. On the seasonal basis, all seasons except winter underestimate the observations and summer shows both the largest mean value (246.7 Wm^{-2}) and underestimation (−6.2 %) (Table 2).

Figure 5 shows that the annual ensemble mean all sky SSR series from ECHAM5-HAM decreases before 1980, increases during the 1980s, and then decreases during the 1990s and 2000s, with a significant negative trend of −0.54 Wm^{-2} $decade^{-1}$ during the 1960–2009 period. All seasonal series show decreasing trends and the variability is similar to the annual series. The largest trends occur in spring (−1.39 Wm^{-2} $decade^{-1}$) (Table 4).

Any potential direct aerosol effect on SSR should be most easily detectable and interpretable under clear-sky condition (Folini and Wild 2011). Figure 6 shows that the annual ensemble mean clear-sky SSR from ECHAM5-HAM decreases before the mid-1970s and after the mid-1980s, and has a significantly decreasing trend of −0.67 Wm^{-2} $decade^{-1}$, which is larger than under all-sky conditions. All seasons have decreasing trends, and the largest trend also occurs in summer (−0.88 Wm^{-2} $decade^{-1}$) (Table 4). Overall, the ensemble mean SSR shows larger trends under clear sky conditions than under all sky conditions, except spring (Table 4).

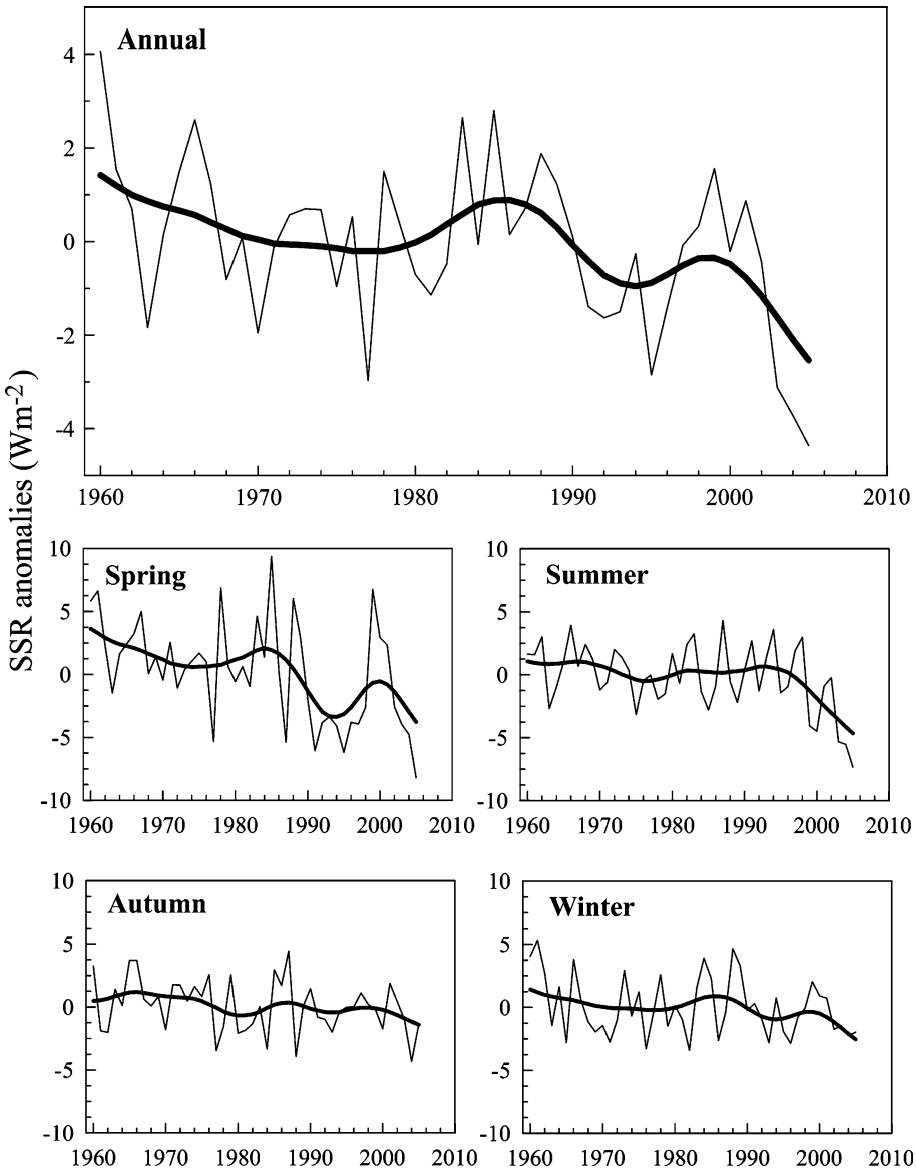

Fig. 5 ECHAM5-HAM simulated mean annual and seasonal all-sky ensemble SSR series (*thin lines*) in the Tibetan Plateau during the period 1960–2005. The series are expressed as differences (anomalies in Wm^{-2}) relative to the 1971–2000 reference period, and are plotted together with a GLPD17 (*thick lines*)

5 Discussion and conclusions

This study analyzed the temporal variability of all-sky and clear-sky surface solar radiation (SSR) data in the eastern and central Tibetan Plateau (TP) during the 1960–2009 period. The results provide observational evidence for an overall decrease of SSR in the TP from 1960 to 2009. The observed decrease is, however, far from linear. Periods of both increasing and decreasing SSR are identified, both under clear sky and all sky conditions. Our results are in line with the all-sky SSR overall decrease observed in China (including a partial recovery in the 1990s) (Che et al. 2005; Liang and Xia 2005; Norris and Wild 2009; Shi et al. 2008; Wild et al. 2009) and India (Kumari et al. 2007; Kumari and Goswami 2010) during the last decades, although the TP shows much smaller amplitudes in the trends. In China, Shi et al. (2008) have shown that the change of direct irradiance is similar to that of global irradiance, with a decreasing trend during 1957–2000, and the most noticeable decrease occurred in the Sichuan and Guizhou area and in the middle and lower reaches of the Yangtze River. In the TP, direct irradiance at most stations shows decreasing trends, varying from −1 to −6 % per decade during the past 40 years. The patterns and magnitudes of trends are consistent with previous studies (Che et al. 2005; Liang and Xia 2005).

Similar conclusions can be reached for clear-sky SSR trends, as a downward trend from the 1960s to the 1990s and a partial recovery thereafter has been observed for the whole China (Liu et al. 2004; Qian et al. 2007; Xia 2010), which is consistent with the clear-sky SSR trends shown in this study before the 2000s. It is noticeable that distinctly

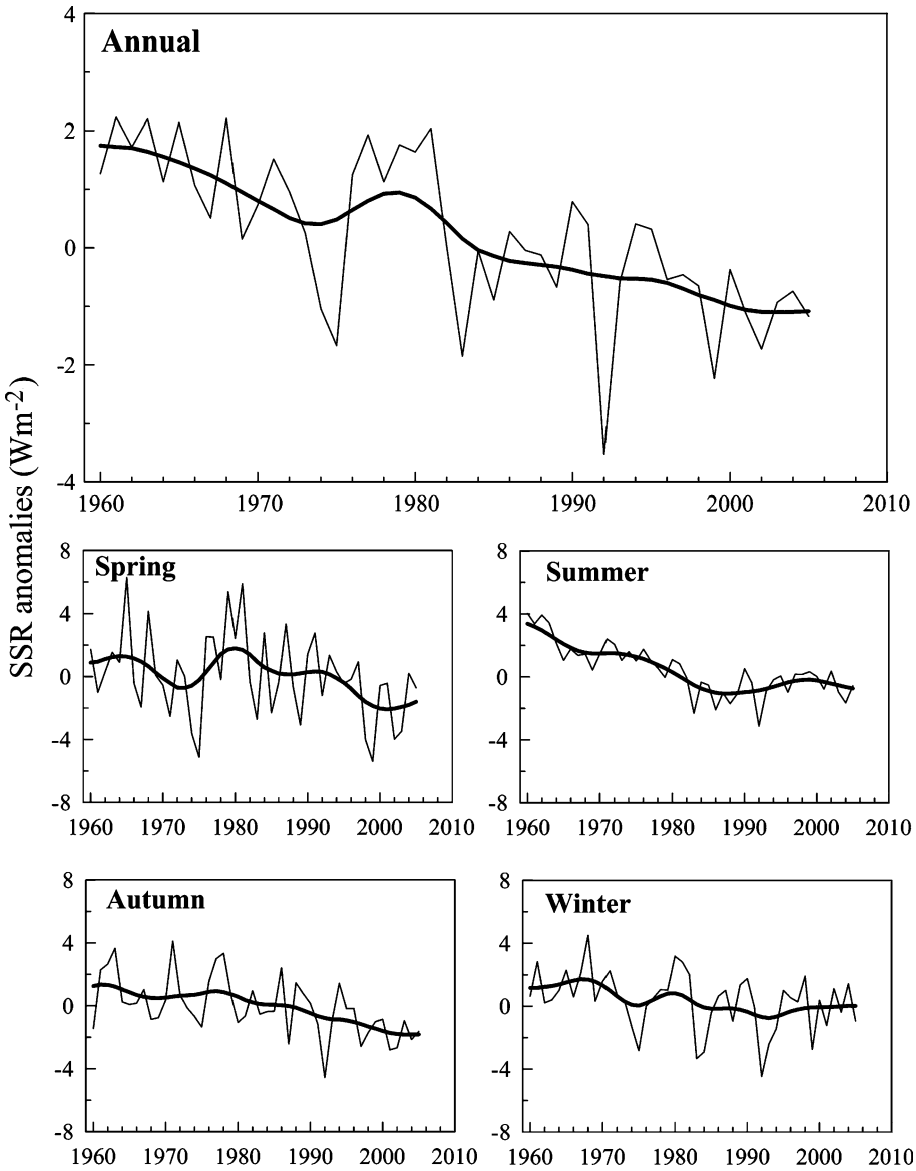

Fig. 6 As Fig. 5, but for clear-sky ensemble SSR series. In order to facilitate the comparison with the clear-sky ensemble SSR observations, only the nearest grid points to the 4 homogeneous stations are considered

Table 4 Linear trends in the mean Tibetan Plateau all-sky and clear-sky ensemble SSR as determined by the ECHAM5-HAM transient simulation, given as Wm^{-2} $decade^{-1}$, considering the 1960–2005 period and two subperiods (before and after 1993)

	Annual	Spring	Summer	Autumn	Winter
ECHAM5-HAM all-sky, 1960–2005	−0.54*	−1.39*	−0.79*	−0.42	−0.42
ECHAM5-HAM all-sky, 1960–1992	−0.27	−1.14*	−0.35	−0.42	−0.21
ECHAM5-HAM all-sky, 1993–2005	−1.71	−0.08	−6.81*	−1.04	−0.04
ECHAM5-HAM clear-sky, 1960–2005	−0.67*	−0.58	−0.88*	−0.70*	−0.44*
ECHAM5-HAM clear-sky, 1960–1992	−0.78*	−0.13	−1.54*	−0.61	−0.71*
ECHAM5-HAM clear-sky, 1993–2005	−1.03*	−1.97	−0.41	−1.77*	+0.80

* Significant at the 0.05 level

low clear-sky SSR anomalies appear around 1963, 1983–1984 and 1992, which occur immediately following to the Agung (1963, Indonesia), El Chichon (1982, Mexico) and Pinatubo (1991, Philippines) volcanic eruptions. These strong decreases detected in the clear-sky SSR series can be the consequence of the direct effect of the

aerosols released by these volcanic eruptions. A strong decrease is also observed in 2004, which cannot be explained by volcanic eruptions but agrees with a sudden increase of aerosols observed in the TP (Luedeling et al. 2011), which is consistent with Xia et al. (2008) based on the satellite AOD retrievals using MISR measurements which indicated that AOD in 2004 is generally larger than the 9-year average. Thus, lower SSR in 2004 is probably associated with larger AOD, possibly as a result of the extraordinary dust storm that occurred in the Gobi desert in 2004 (Qu et al. 2006). Whether the sources of dust come from local emission or long-range transportation are unclear in 2004.

In order to learn more about the causes of the TP dimming, we first note that neither NCEP/NCAR nor ERA-40 reanalysis data are able to capture the observed SSR decrease. Although both reanalyses assimilate a comprehensive amount of weather data which constrains the simulated atmospheric states, they cannot reproduce the decadal variations in the all-sky and clear-sky SSR. Inaccurate representation of clouds and the neglect of time varying aerosols in the reanalysis assimilation model are considered as the most likely cause of this disagreement with surface observations (Wild and Schmucki 2011; Xia et al. 2006, 2008). Note that there are differences between the observations, NCEP/NCAR, ERA-40 and ECHAM-HAM with respect to the mean SSR patterns, although ECHAM-HAM can simulate the dimming of SSR shown by observations. This can be caused by the insufficient absorption of solar irradiance in the parameterization in the reanalysis and numerical modes. This is consistent with the previous finding by Wild (2001). Wild (2001) showed that the atmosphere in both NCEP/NCAR and in many GCMs is significantly too transparent for SSR, leading to excessive insolation at the surface. The same should be applied under cloud-free conditions (Wild et al. 2006).

In contrast, transient simulations with ECHAM5-HAM show an overall dimming of annual mean SSR from 1960 to 2005 at a statistically significant level under both all-sky and clear-sky conditions, in line with observational evidence. Correlations between observed and modelled (ensemble mean) annual and seasonal mean all-sky and clear-sky SSR time series smoothed with the 17GLPF range from 0.3 to 0.8 (see Table 5). Differences between observed and modelled SSR exist, however, for some seasons and with regard to the absolute magnitudes of the trends. Despite these shortcomings, the ECHAM5-HAM simulations further support the hypothesis that the dimming observed in the TP is caused by increased aerosol emissions in the TP or in the surrounding regions. The model simulations calculate an almost linear increase in 550 nm AOD over the TP from 1960 to 2005 (Fig. 7), in line with the linear decrease in clear-sky SSR. The correlations between SSR and AOD series (Table 5) provide values of −0.72 and −0.81 for the smoothed annual series of all-sky and clear-sky SSR series, respectively. High correlations are also found on a seasonal basis, especially during autumn. Whether the source of these aerosols lies in the TP or in surrounding regions remains a subject for future studies, as for example with the help of dedicated sensitivity experiments.

Compared with other regions, the TP should be regarded as a region with clear atmospheric condition. Taking Nam Co in the central TP as an example, the baseline AOD of Nam Co is 0.029, which is about half of that over the Pacific Ocean and the Atlantic Ocean (Xia et al. 2011). At the same time, aerosol radiative effects are exponentially correlated with AOD. This suggests that the TP is sensitive to aerosol direct and indirect radiative effects and an equivalent increase of AOD here can produce much larger aerosol direct and indirect effects as compared with regions with larger background AOD. This hypothesis has been supported by the evidence that the atmospheric brown clouds (mostly as a result of biomass burning and fossil fuel consumption) can amplify the warming in the TP and may account for the observed retreat of Himalayan glaciers (Ramanathan et al. 2007). On the other hand, black soot aerosols deposited on glaciers in the TP significantly contribute to the rapid glacier retreat (Xu et al. 2009).

However, one may speculate that the sources of these aerosols have a large-scale rather than a local origin, which has been a hot topic in recent years (e.g. Xu et al. 2009; Xia

Table 5 Correlation coefficients between the mean all-sky and clear-sky GLPF17 series from observed SSR and ECHAM5-HAM transient simulations in the Tibetan Plateau on the annual and seasonal basis

	Annual	Spring	Summer	Autumn	Winter
Observed all-sky SSR					
ECHAM5-HAM all-sky SSR	0.31	−0.28	0.43	0.68	0.59
ECHAM5-HAM clear-sky SRR	0.59	−0.59	0.52	0.89	0.64
ECHAM5-HAM AOD	−0.72	0.33	−0.60	−0.84	−0.54
Observed clear-sky SSR					
ECHAM5-HAM all-sky SSR	0.30	−0.06	0.31	0.79	0.36
ECHAM5-HAM clear-sky SSR	0.71	−0.12	0.39	0.85	0.84
ECHAM5-HAM AOD	−0.81	−0.40	−0.38	−0.90	−0.93

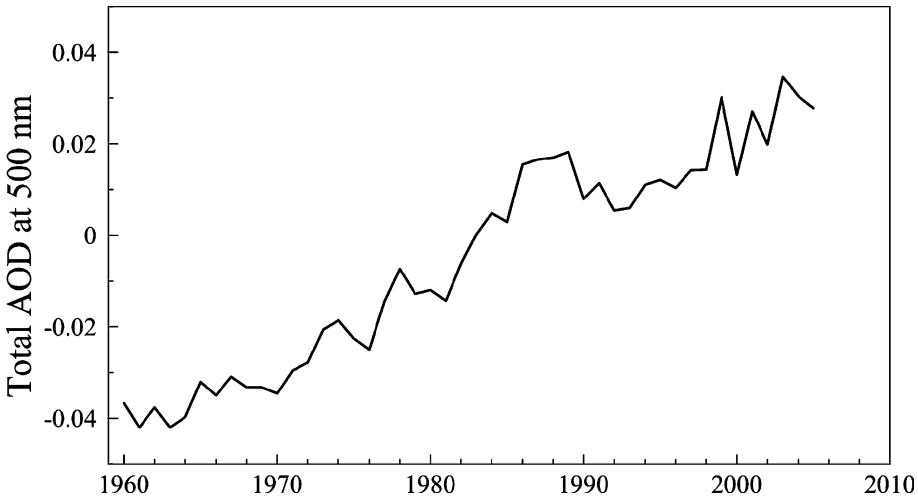

Fig. 7 ECHAM5-HAM simulated mean annual aerosol optical depth (AOD) at 550 nm in the Tibetan Plateau during the period 1960–2005. The series are expressed as differences (anomalies) relative to the 1971–2000 reference period, and are calculated using the nearest grid points to the 10 surface stations with all-sky SSR series

et al. 2008; Kopacz et al. 2011). Based on the back-trajectory analysis, Lu et al. (2012) found that the black carbon in the TP has increased by 41 % during 1961–2010, and South Asia and East Asia are the two main source regions, accounting for 67 and 17 % of black carbon transported to the TP on an annual basis. This is slightly different from Kopacz et al. (2011), suggesting that the TP receives most black carbon from western and central China, as well as from India, Nepal, the Middle East, Pakistan and other countries. The south westerly winds associated with the Indian summer monsoon may lead to some exports of Indian aerosol to the TP. However, the contributions of different source regions transported to the TP vary with season and location (Xia et al. 2011; Lu et al. 2012). The rather steady decrease of observed and modelled SSR in the TP in summer may be partly attributable to increasing Indian aerosol emissions, although the amounts of anthropogenic aerosol such as black carbon reaching the TP in summer are lower than that in winter (Lu et al. 2012). Other sources of aerosols transported to the TP in summer cannot be ruled out. For example, dust transportation from Taklimakan Desert to the TP mainly occurs in summer (Xia et al. 2008). In the winter half year, prevailing winds are rather from the north, i.e. from the desert regions north of the TP, and consequently a predominant influence of the desert dust is a possible cause of the decreasing SSR in the TP in winter.

Furthermore, it cannot be excluded that the observed SSR trends in the TP are affected by the increasing local aerosol emissions (Qian et al. 2006, 2007; Kaiser and Qian 2002), e.g. connected with heating, despite the scarcity of population in the region. In fact, the industrial waste gas and soot emissions and number of civilian vehicles in the Tibet have been increasing in the last decades, especially after the 1980s (e.g. see statistics in You et al. (2010b)). This increase of anthropogenic activities would imply a rapid increase in the emissions of aerosol in the TP, although at a lower rate than in East China and India.

In conclusion, as in many other parts around the globe, an overall decrease in SSR has been documented in the TP since the 1960s, based on both observational and modelling approaches. This decrease is found under both all sky and clear sky conditions and seems to be related to increasing aerosols emissions during the last decades, as has been shown by the simulations performed with the ECHAM5-HAM global climate model. However, further research is needed in order to better assess the origin of the aerosols over the TP.

Acknowledgments This study has been supported by the Global Change Research Program of China (2010CB951401), the Chinese Academy of Sciences (KZCX2-YW-145), and the National Natural Science Foundation of China (40870743). It became possible through a Sino-Swiss Science and Technology Cooperation (SSSTC) research grant (EG76-032010 and EG23-092011). The China postdoctoral science foundation (the 49th) is also appreciated. The authors thank the National Meteorological Information Center, China Meteorological Administration (NMIC/CMA), for providing the data for this study. Qinglong You is supported by the Alexander von Humboldt Foundation. Arturo Sanchez-Lorenzo is supported by a postdoctoral fellowship from the "Comissionat per a Universitats i Recerca del Departament d'Innovació, Universitats i Empresa de la Generalitat de Catalunya" (2009 BP-A 00035). ECHAM5-HAM simulations were carried out at the Swiss National Supercomputing Center (CSCS). We are very grateful to the reviewers for their constructive comments and thoughtful suggestions.

References

Roeckner E et al (2003) The atmospheric general circulation model ECHAM5. Part I: model description. Hamburg: Max-Planck-Institute for Meteorology MPI Report No. 349

Sanchez-Lorenzo A et al (2009) Dimming/brightening over the Iberian Peninsula: Trends in sunshine duration and cloud cover and their relations with atmospheric circulation. J Geophys Res 114: D00D09

Wild M et al (2009) Global dimming and brightening: an update beyond 2000. J Geophys Res 114:D00D13
Alexandersson H, Moberg A (1997) Homogenization of Swedish temperature data 1. Homogeneity test for linear trends. Int J Climatol 17(1):25–34
Barnett TP et al (2005) Potential impacts of a warming climate on water availability in snow-dominated regions. Nature 438:303–309
Bichet A et al (2011) Global precipitation response to changing external forcings since 1870. Atmos Chem Phys 11:9961–9970
Cha LS (1996) A study on spatial and temporal variation of solar radiation in China (in Chinese). Sci Geograph Sin 16:232–237
Che HZ et al (2005) Analysis of 40 years of solar radiation data from China, 1961–2000. Geophys Res Lett 32:L06803
Folini D, Wild W (2011) Aerosol emissions and dimming/brightening in Europe: sensitivity studies with ECHAM5-HAM. J Geophys Res 116:D2114
Gilgen H et al (1998) Means and trends of shortwave irradiance at the surface estimated from GEBA. J Clim 11:2042–2061
Immerzeel WW et al (2010) Climate change will affect the Asian Water Towers. Science 328(5984):1382–1385
Kaiser DP, Qian Y (2002) Decreasing trends in sunshine duration over China for 1954–1998: indication of increased haze pollution? Geophys Res Lett 29:2042
Kalnay E et al (1996) The NCEP/NCAR 40-year reanalysis project. Quart J Roy Meteor Soc 77(3):437–471
Kang SC et al (2010) Review of climate and cryospheric change in the Tibetan Plateau. Environ Res Lett 5(1):015101
Kopacz M et al (2011) Origin and radiative forcing of black carbon transported to the Himalayas and Tibetan Plateau. Atmos Chem Phys 11:2837–2852
Kumari BP, Goswami BN (2010) Seminal role of clouds on solar dimming over the Indian monsoon region. Geophys Res Lett 37:L06703
Kumari BP et al (2007) Observational evidence of solar dimming: offsetting surface warming over India. Geophys Res Lett 34:L21810
Li XW et al (1998) Analysis of the solar radiation variation of the China in recent 30 years (in Chinese). Quart J Appl Meteor 9:24–31
Liang F, Xia XA (2005) Long-term trends in solar radiation and the associated climatic factors over China for 1961–2000. Ann Geophys 23(7):2425–2432
Liepert BG (2002) Observed reductions of surface solar radiation at sites in the United States and worldwide from 1961 to 1990. Geophys Res Lett 29(10):1421
Liu B et al (2004) Taking China's temperature: daily range, warming trends, and regional variations, 1955–2000. J Clim 17:4453–4462
Lohmann U et al (2007) Cloud microphysics and aerosol indirect effects in the global climate model ECHAM5-HAM. Atmos Chem Phys 7:3425–3446
Lu Z et al (2012) A novel back-trajectory analysis of the origin of black carbon transported to the Himalayas and Tibetan Plateau during 1996–2010. Geophys Res Lett 39:L01809
Luedeling E et al (2011) Replies to Shen, Chen et al. and Yi and Zhou: linear regression analysis misses effects of winter temperature on Tibetan vegetation. Proc Natl Acad Sci USA 108(19):E95
Norris JR, Wild M (2009) Trends in aerosol radiative effects over China and Japan inferred from observed cloud cover, solar "dimming,'' and solar "brightening''. J Geophys Res 114: D00D15
Ohmura A (2009) Observed decadal variations in surface solar radiation and their causes. J Geophys Res 114:D00D05
Qian Y et al (2006) More frequent cloud-free sky and less surface solar radiation in China from 1955 to 2000. Geophys Res Lett 33:L01812
Qian Y et al (2007) Variability of solar radiation under cloud-free skies in China: the role of aerosols. Geophys Res Lett 34:L12804
Qu JJ et al (2006) Asian dust storm monitoring combining terra and aqua MODIS SRB measurements. IEEE Geosci Remote Sens 3(4):484–486
Ramanathan V et al (2007) Warming trends in Asia amplified by brown cloud solar absorption. Nature 448:575–578
Rayner NA et al (2003) Global analyses of sea surface temperature, sea ice, and night marine air temperature since the late nineteenth century. J Geophys Res 108:4407
Roeckner E et al (2006) Sensitivity of simulated climate to horizontal and vertical resolution in the ECHAM5 atmosphere model. J Clim 19(16):3771–3791
Sen PK (1968) Estimates of regression coefficient based on Kendall's tau. J Am Stat Assoc 63:1379–1389
Shi GY et al (2008) Data quality assessment and the long-term trend of ground solar radiation in China. J Appl Meteorol Climatol 47(4):1006–1016
Solanki SK, Krivova NA (2003) Can solar variability explain global warming since 1970? J Geophys Res 108:1200
Stanhill G, Cohen S (2001) Global dimming: a review of the evidence for a widespread and significant reduction in global radiation with discussion of its probable causes and possible agricultural consequences. Agric For Meteorol 107(4):255–278
Stier P et al (2006a) Emission-induced nonlinearities in the global aerosol system: results from the ECHAM5-HAM aerosol-climate model. J Clim 19(16):3845–3862
Stier P et al (2006b) The evolution of the global aerosol system in a transient climate simulation from 1860 to 2100. Atmos Chem Phys 6:3059–3076
Tang WJ et al (2010) Quality control and estimation of global solar radiation in China. Sol Energy 84:466–475
Tang WJ et al (2011) Solar radiation trend across China in recent decades: a revisit with quality-controlled data. Atmos Chem Phys 11:393–406
Uppala SM et al (2005) The ERA-40 re-analysis. Q J R Meteorol Soc 131(612):2961–3012
Vincent LA et al (2005) Observed trends in indices of daily temperature extremes in South America 1960–2000. J Clim 18(23):5011–5023
Wang CH et al (2011) Factors affecting the surface radiation trends over China between 1960 and 2000. Atmos Environ 45:2379–2385
Wild M (2001) Surface and atmospheric radiation budgets as determined in reanalyses. Irs 2000: current problems in atmospheric radiation, pp 602–605
Wild M (2009) Global dimming and brightening: a review. J Geophys Res 114: D00D16
Wild M, Schmucki E (2011) Assessment of global dimming and brightening in IPCC-AR4/CMIP3 models and ERA40. Clim Dyn 37:1671–1688
Wild M et al (2005) From dimming to brightening: decadal changes in solar radiation at earth's surface. Science 308(5723):847–850
Wild M et al (2006) Evaluation of clear-sky solar fluxes in GCMs participating in AMIP and IPCC-AR4 from a surface perspective. J Geophys Res 111:D01104
Xia XA (2010) A closer looking at dimming and brightening in China during 1961–2005. Ann Geophys 28(5):1121–1132
Xia XA et al (2006) Analysis of down welling surface solar radiation in China from National Centers for Environmental Prediction reanalysis, satellite estimates, and surface observations. J Geophys Res 111:D09103

Xia XA et al (2008) Aerosol optical depth over the Tibetan Plateau and its relation to aerosols over the Taklimakan Desert. Geophys Res Lett 35:L16804

Xia XA et al (2011) Baseline continental aerosol over the central Tibetan plateau and a case study of aerosol transport from South Asia. Atmos Environ 45:7370–7378

Xu XD et al (2008) World water tower: an atmospheric perspective. Geophys Res Lett 35:L20815

Xu BQ et al (2009) Black soot and the survival of Tibetan glaciers. Proc Natl Acad Sci USA 106:22114–22118

You QL et al (2008a) Changes in daily climate extremes in the eastern and central Tibetan Plateau during 1961–2005. J Geophys Res 113:D07101

You QL et al (2008b) Relationship between trends in temperature extremes and elevation in the eastern and central Tibetan Plateau, 1961–2005. Geophys Res Lett 35:L04704

You QL et al (2010a) Decreasing wind speed and weakening latitudinal surface pressure gradients in the Tibetan Plateau. Clim Res 42(1):57–64

You QL et al (2010b) From brightening to dimming in sunshine duration over the eastern and central Tibetan Plateau (1961–2005). Theor Appl Climatol 101(3–4):445–457

You QL et al (2010c) Climate warming and associated changes in atmospheric circulation in the eastern and central Tibetan Plateau from a homogenized dataset. Glob Planet Change 72(1–2):11–24